J Opt
https://doi.org/10.1007/s12596-024-01736-x

RESEARCH ARTICLE

Structural, optical and electrical properties of In_2O_3/α-Fe_2O_3 heterostructure thin films for photocatalytic application

A. Arfaoui[1]

Received: 28 November 2023 / Accepted: 9 February 2024

Abstract In this study, In_2O_3/α-Fe_2O_3 heterostructure thin film was prepared on glass substrate using a low-cost and simple spray pyrolysis technique. After successful deposition, the structure and morphology were investigated by X-ray diffraction, scanning electron microscopy, EDX and Raman microscopy. The X-ray diffraction studies confirm the rhombohedral phase of α-Fe_2O_3 and the cubic phase of In_2O_3 without other impurity peaks, this result also was proved by Raman spectroscopy. The surface morphology of In_2O_3/α-Fe_2O_3 thin film was determined by using scanning electronic microscopy (SEM), which indicates the formation of a very homogenous surface with a spherical grain randomly disturbed with diverse sizes. Hall effect measurements showed that the conduction of In_2O_3/α-Fe_2O_3 was n type, and the most electrons are free charge carriers. The resistivity, hall mobility and charge carriers concentration are equal to 5.7×10^{-4} Ω cm, 5.82 cm^2/V S and 1.87×10^{21} cm^{-3}, respectively. On the other hand, the grain size was equal to 28.2 nm for In_2O_3 and 30.61 for In_2O_3/α-Fe_2O_3 thin films. The prepared In_2O_3/α-Fe_2O_3 thin film was used as a photocatalyst against methylene blue, and this layer demonstrates significantly higher photocatalytic efficiency with degradation rate compared to In_2O_3 thin layer which may be related to the surface roughness and crystallite size measured by XRD and SEM.

Keywords In_2O_3/α-Fe_2O_3 thin film · Spray pyrolysis · Structural study · EDX · Raman microscopy · Hall effect · Photocatalytic activity

✉ A. Arfaoui
aarfaoui@ju.edu.sa

[1] Department of Physics, College of Science, Jouf University, P. O. Box 2014, Sakaka, Saudi Arabia

Introduction

The utilization of solar energy has gained attention recently since it is a sizable, sustainable and clean energy source. The effective exploitation of this energy will offer enough power to fulfill the rising global energy demand. Additionally, solar energy can be used for organic synthesis and environmental cleanup. Of all the options for converting solar energy, photoelectrochemical water decomposition is the most convincing strategy for producing clean and renewable fuels. Due to their stability, natural abundance and suitable band gap that makes use of 40% of electromagnetic radiation, In_2O_3 and Fe_2O_3 have been viewed as an appealing alternative among the many semiconducting materials for photocatalytic application [1, 2].

First of all, In_2O_3 may be made into an n-type semiconductor with a high electrical conductivity. It is a transparent semiconductor with a moderate band gap of 2.8 eV. It also crystallizes in a cubic bixbyite structure and has a transparent nature. Due to its low cost, stable physicochemical and visible light responsive properties, this material has attracted a lot of attention in the photocatalytic destruction of organic contaminants and photo-splitting of water. It is well known that In_2O_3, either on its own or in combination with other oxides of transition metals, became the most widely used transparent conducting oxide (TCO) in photocatalytic and related applications. Previous research suggests that the strong visible light harvesting capacity and the efficient spatial separation of photogenerated electron hole pairs in In_2O_3, when combined with other semiconductors, improve the photocatalytic efficiency [3].

Iron oxide Fe_2O_3, on the other hand, is a conventional form of sensing and has been studied because of its high sensitivity, rapid response, as well as durability. It is also a typical n-type semiconductor with a band gap of 2.1 eV.

Published online: 02 April 2024

However, only a small number of studies have taken into account the development of a heterojunction system based on In_2O_3 and Fe_2O_3 for photocatalytic application [4, 5].

In order to improve the performance of acetone sensing, Zhang et al. have recently revealed simple techniques to create Fe_2O_3–In_2O_3 heterostructure nanocomposites. The resulting samples showed good qualities such as a strong response and recovery capacities.

Additionally, the investigation of the Hall effect enables the determination of the concentration and mobility of charge carriers as well as, in some cases, the intrinsic energy gap and crucial data on the electrical characteristics of semiconductors [6].

In this work, we prepared In_2O_3 thin films on glass substrate using the spray pyrolysis technique. Fe_2O_3 was subsequently grown on the In_2O_3 to form heterojunction structure. The phase structure, morphologies, Hall effect and photocatalytic performance of the resultant samples were carried out.

Experimental

Film preparation

In_2O_3 thin film preparation

In_2O_3 thin film was prepared by spraying an aqueous solution of indium chloride ($InCl_3$). The concentration of indium chloride is 0.01 M. This solution was sprayed under N_2 gas pressure of 0.5 bar on glass substrates, which were placed on hot plate heated at 350 °C.

In_2O_3/α-Fe_2O_3 thin film preparation

After preparing In_2O_3 thin films, α-Fe_2O_3 thin film was prepared from aqueous solution containing Iron(III) chloride dehydrate ($FeCl_3 \cdot 2H_2O$) with concentration equal to 10^{-2} M as a precursor using spray pyrolysis technique on the In_2O_3 substrates at a temperature equal to 350 °C.

Characterization techniques

The spectra of X-ray diffraction of obtained thin films were examined using Cu K_α radiation ($\lambda = 0.15418$ nm) and a copper-source diffractometer (Analytical X Pert PROMP D), with 2θ varying from 0° to 70°. The micro-Raman system from Jobin Yvon Horibra LABRAM-HR, which is visible between 200 and 1200 cm^{-1}, was used to record Raman scattering studies at room temperature. In addition, A JEOL-JSM 5400 model scanning electron microscope (SEM) was used to examine the morphology of the films. For elemental analysis with an electron gun, an energy-dispersive X-ray (EDX) spectrometer coupled to a thermal field emission scanning electron microscope was employed. A Hall measuring system using the van der Pauw method was used to conduct electrical tests, resistivity, Hall mobility and carrier concentration at room temperature with a mild magnetic field of approximately 0.554 T.

Finally, the breakdown rate of methylene blue (MB) aqueous solution under solar illumination was used to determine the photocatalytic activity of the structures based on In_2O_3 and In_2O_3/Fe_2O_3 thin films. MB was initially present in a concentration of 4.5 mg/L. For one hour in the dark, the MB solution was agitated at a magnetic stirrer to achieve equilibrium adsorption. In_2O_3 and In_2O_3/Fe_2O_3 thin films served as photocatalysts in the aqueous solution of MB, which was continuously stirred while exposed to sunlight. Analytical samples were taken from the solution every 1, 2, 3, 4, 5 and 6 h to determine the impact of sun light irradiation on MB solution, and a UV–Vis spectrophotometer was used to determine the amount of MB present in each sample.

The efficiency of MB degradation was calculated based on the following equation:

$$\text{Degradation efficiency}(\%) = \left(\frac{A_0 - A}{A_0} \times 100\right) = \left(\frac{C_0 - C}{C_0} \times 100\right) \quad (1)$$

where A_0, A, C_0 and C are the absorbance and concentration of MB corresponding to the initial time and the variable time, respectively.

Results and discussion

XRD analysis

Figure 1 shows the XRD patterns obtained for the pure In_2O_3, pure α-Fe_2O_3 and In_2O_3/α-Fe_2O_3 heterostucture thin film. The primary diffraction peaks for the In_2O_3 thin films were consistent with the conventional cubic structure represented by JCPDS card number 06-0416. These peaks demonstrate the synthesis of the pure phase In_2O_3 [7, 8]. In addition, the XRD pattern obtained for the α-Fe_2O_3 thin films showed the presence of Rhombohedral structure according to the standard card for Fe_2O_3 (JCPDS No. 01-1053) Fig. 1b. Finally, Fig. 1c presents the X-ray pattern of In_2O_3/α-Fe_2O_3 where the main diffraction peaks correspond to the Rhombohedral phase of α-Fe_2O_3 (JCPDS No. 01-1053) and the cubic phase of In_2O_3 (JCPDS No. 06-0416). There were no further impurity peaks or mixed oxides, proving that there was no chemical interaction between the various metal oxides [9].

Debye–Scherrer's equation, which is given in Eq. 2, can be used to determine the average value of In_2O_3/α-Fe_2O_3 thin films crystallite size [4]:

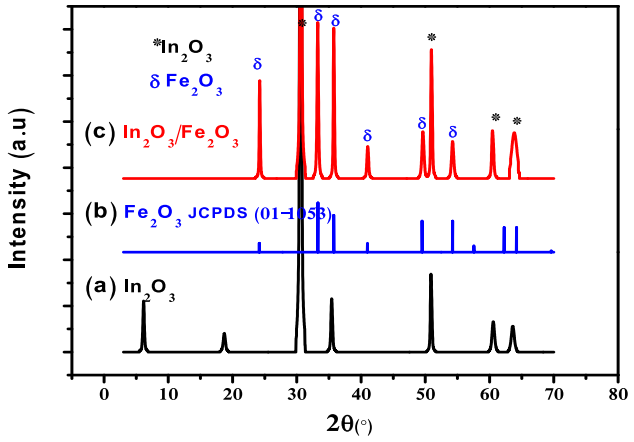

Fig. 1 X-ray diffractogram of **a** In_2O_3, **b** α-Fe_2O_3 and **c** In_2O_3/α-Fe_2O_3 heterostructure thin films

$$D = \frac{K\lambda}{\beta \cos\theta} \tag{2}$$

where K is Scherrer's constant equal to 0.9, λ is the wavelength of incident beam, β is the width at half height intensity or full width half maximum of the peak and θ represents the diffraction angle. The average crystallite size was 28.2 nm for In_2O_3 and 30.61 for In_2O_3/α-Fe_2O_3 thin films. The larger radius of In^{3+}, which has five layers of electrons as opposed to four layers for Fe^{3+}, can be attributed to the Debye–Scherrer Formula's rule that a narrower peak results in a bigger grain size. As a result, In_2O_3 has a wider radius than Fe_2O_3, and the little amount of In^{3+} that is replaced by Fe^{3+} results in a reduction in the size of the average unit cell. Due to these factors, In_2O_3/α-Fe_2O_3 thin film has higher average grains than In_2O_3 [5].

In the same vein, the relationship shown below was used to compute the microstrain ($\boldsymbol{\varepsilon_{str}}$) that was generated in these thin films:

$$\varepsilon_{str} = \frac{\beta \cos\theta}{4} \tag{3}$$

This strain, which is of order 10^{-3}, is caused by a tensile stress that due to In^{3+} ions substitution by Fe^{3+} ions in the lattice. Table 1 presents the estimated grain sizes $\boldsymbol{D}$ as well as the microstrain ($\boldsymbol{\varepsilon_{str}}$) for various thin films.

Table 1 The grain size and the microstrain of In_2O_3, α-Fe_2O_3 and In_2O_3/α-Fe_2O_3 thin films

Samples	In_2O_3	In_2O_3/α-Fe_2O_3	α-Fe_2O_3
The grain size $\boldsymbol{D}$ (nm)	28.2	30.61	38.11
Strain $\boldsymbol{\varepsilon_{str}}$ (10^{-3})	1.23	1.13	0.91

Raman measurements

In order to investigate the crystal structure and identify the structure of thin films, Raman spectrum was performed on the In_2O_3/α-Fe_2O_3 thin films as presented in Fig. 2.

The peaks at 243, 292, 404 and 604 cm^{-1} belong to Eg modes of α-Fe_2O_3, while peaks at 221 and 497 cm^{-1} relate to A1g modes. These findings supported the creation of pure Fe_2O_3, while the vibrational modes at 507 cm^{-1} belonged to In_2O_3 [10–12].

EDX measurments

The mapping pattern for the acquired thin films is shown in Fig. 3. The spectrum for these films indicates that they only contained the three components O, Fe and In. No other elements were found in the films, which were made of the material In_2O_3/α-Fe_2O_3. In contrast to the Fe and O signals, which were evenly distributed throughout the whole structure, the In signals were primarily discovered in the core region and only rarely in the outside region. These findings supported the distinctive quality of heterostructure nanocomposites. No other elements could be detected within the sensitivity of the apparatus indicating high purity of In_2O_3/α-Fe_2O_3 thin films which is consistent with the results reported in the earlier literature [11–13].

Morphological properties

The surface morphologies of In_2O_3/α-Fe_2O_3 thin film were determined using scanning electronic microscopy (SEM) and presented in Fig. 4. The SEM images show the development of a fairly homogeneous surface with a spherical grain that is randomly disturbed and has a various of sizes. This surface disturbance is may be caused by very tiny droplets from the spray process that evaporate above the glass substrates and condense as microcrystallites of different sizes.

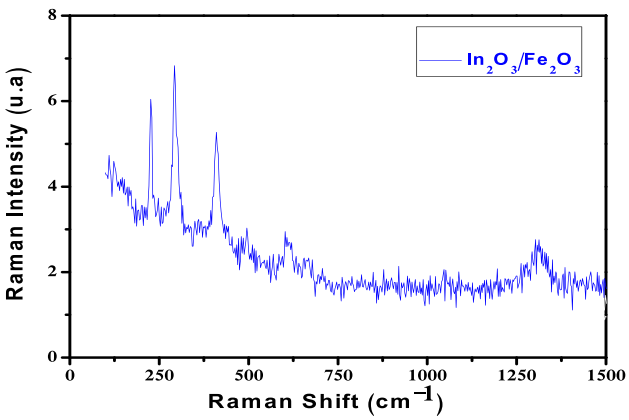

Fig. 2 The Raman spectra of In_2O_3/α-Fe_2O_3thin films

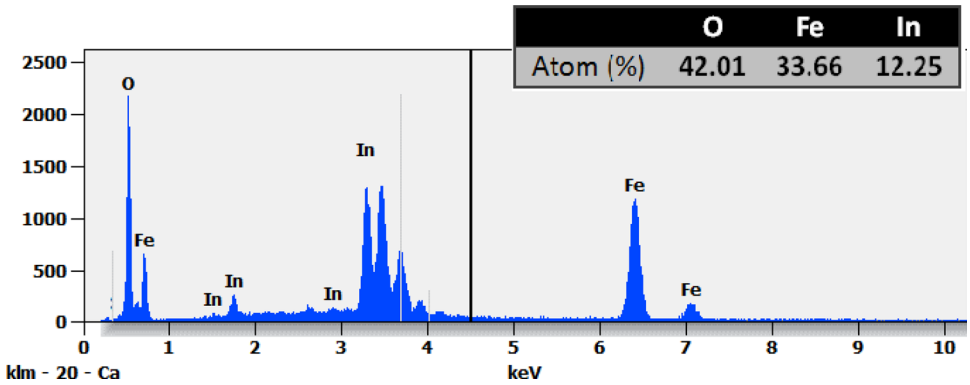

Fig. 3 EDX spectra from In_2O_3/α-Fe_2O_3thin film

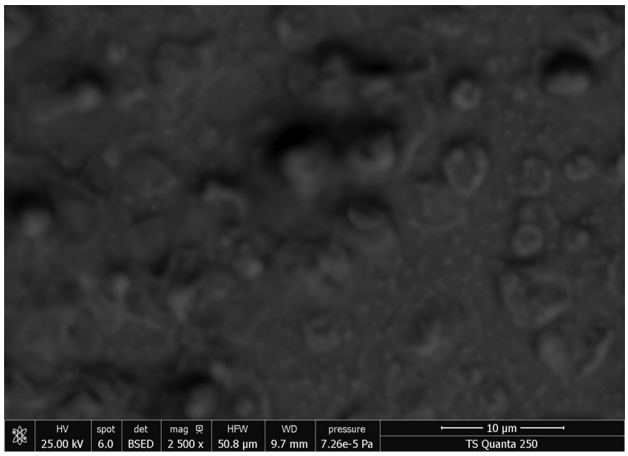

Fig. 4 SEM micrographs of In_2O_3/α-Fe_2O_3 thin films

Table 2 Electrical resistivity ρ, the Hall mobility μ and charge carriers concentration n of In_2O_3/α-Fe_2O_3 thin films

Conductivity-type	Resistivity ρ (10^{-4} Ω cm)	μ (cm^2/V S)	Carrier concentration n (10^{20} cm^{-3})
n	5.71	5.82	− 18.7

Hall effect study

At room temperature, the electrical characteristics of In_2O_3/α-Fe_2O_3 thin films were assessed using the Hall effect. Charge carrier concentration, Hall mobility and electrical resistivity dependency are summarized in Table 2.

Hall measurements show the degenerate n-type semiconductors in the thin layer [14], and the majority of free charge carriers are electrons. Charge carriers concentration, resistivity and Hall mobility are equal to 5.7×10^{-4}Ω cm, 5.82 cm^2/V S and -18.7×10^{20} cm^{-3}, respectively.

Photocatalytic test

Indium oxide has attracted a lot of attention as a semiconductor photocatalyst because it has demonstrated considerable potential for minimizing energy and environmental issues during the past few decades. To create novel photocatalysts with even improved performance, different photocatalyst systems based on indium oxide heterojunctions have been developed [15–17]. Numerous experiments have been done to alter In_2O_3 thin films to enhance their photocatalytic activity, improve their optical characteristics and extend the absorption edge to visible light. The process of coupling two semiconductors involves combining semiconductor metal oxides, such as In_2O_3/α-Fe_2O_3 has been studied for surface and optical modification, and in this work, we studied the effect In_2O_3/α-Fe_2O_3 heterojunction thin films on the degradation of MB under sun light. Wherefore, a notable way to encourage the migration of photoexcited electrons and holes and to lower its band gap is by combining metal oxides with α-Fe_2O_3 host. The photo-induced holes on α-Fe_2O_3 with higher valence band potential will combine with the photo-induced electrons on In_2O_3 with lower conduction band potential, while the stronger redox-capable electrons and holes remain on α-Fe_2O_3 and, respectively [18].

In addition, the formation of In_2O_3/α-Fe_2O_3 heterojunction can efficiently encourage the separation of photoexcited electron–hole pairs and the interfacial charge transfer; additionally, the appropriate arrangement of combined semiconductors' conduction band (CB) levels can encourage the migration of photoexcited electrons. The CB of In_2O_3 (E_{CB} for $In_2O_3 = -0.67$ V vs. NHE) is lower than that of α-Fe_2O_3 (E_{CB} for α-$Fe_2O_3 = 0.32$ V vs. NHE). Thus, when In_2O_3 and α-Fe_2O_3 are coupled together, the heterostructure that is generated is an effective junction to facilitate the separation of photo-induced electron–hole pairs [19].

When an active light source and a photocatalyst are present, photocatalytic activity is crucial for the breakdown and elimination of organic pollutants. It depends on an electrical phenomenon that takes place on a catalyst's surface. According to earlier investigations [20], the potential

dye degradation mechanism of In_2O_3/α-Fe_2O_3 thin films can be viewed in the following ways. Under solar radiation, In_2O_3/α-Fe_2O_3 absorbs an effective photon, which causes the production of electron–hole pairs. The oxygen radical anion $O_2^{\cdot}$ is created when these charge carriers are moved to the catalyst surface, where the electrons they produce are absorbed by O_2 molecules, although surface-bound entities have imprisoned the holes H_2O to produce hydroxyl radicals, $OH^{\cdot}$. The generated radical species ($O_2^{\cdot}$ and $OH^{\cdot}$) aid in the degradation of the organic MB dyes [11]. The color of the MB dye solution quickly disappears when our thin layer is present. Figure 5 explains this technique in more detail.

The thin film capacity increases with dye concentration, which might be explained by a higher probability of MB molecules filling the active groups and resting on the thin film active sites given a constant volume of MB solution and adsorbent. The progressive transformation of the aqueous solution from dark blue to light blue may be detected in various stages of the layers' adsorption of MB.

The photocatalytic activity of In_2O_3/α-Fe_2O_3 thin films was assessed using the degradation of methylene blue (MB) dye under sunlight irradiation for 1–2 h Fig. 6.

Figure 7 shows that when compared to In_2O_3 thin films, In_2O_3/α-Fe_2O_3 has the best photocatalytic degradation of MB. This improvement is likely brought about by the surfaces effect and the large crystallite size discovered by SEM analysis. As a result, the thin films photocatalytic activity will be greatly influenced by its surface properties. This study found that thin films of In_2O_3/α-Fe_2O_3 showed good photocatalytic activity, which may have been impacted by the surface roughness and larger particle size.

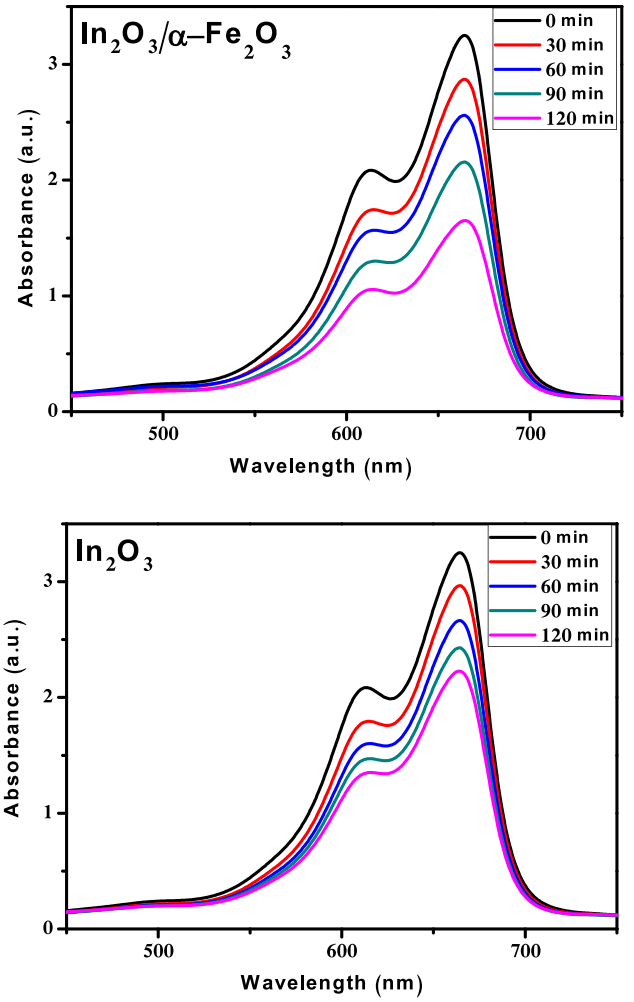

Fig. 6 Absorption spectra of MB showing its degradation by In_2O_3 and In_2O_3/α-Fe_2O_3 thin film under solar radiation

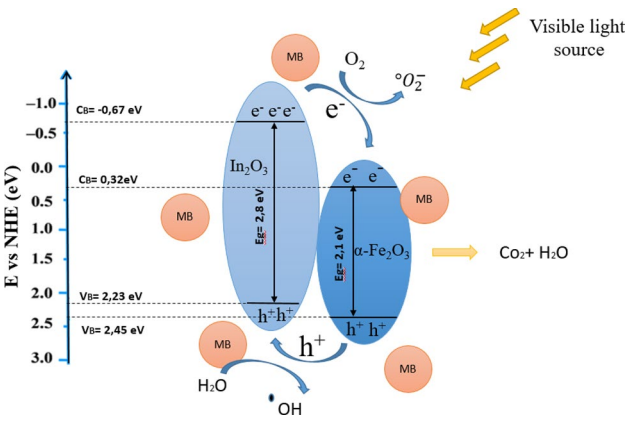

Fig. 5 Diagram showing the mechanism of photocatalytic degradation of MB by In_2O_3/α-Fe_2O_3 thin films

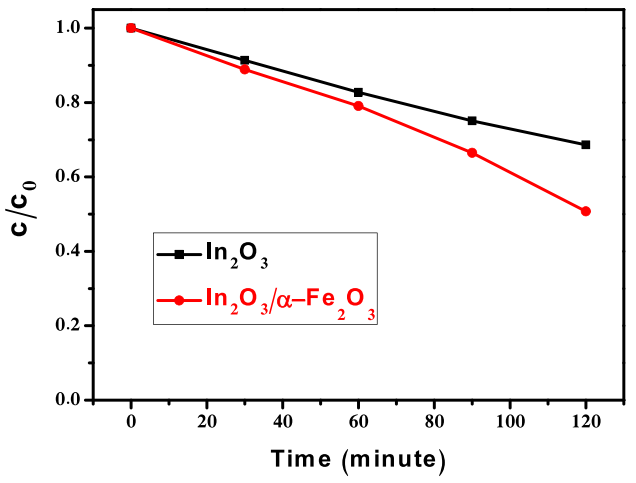

Fig. 7 Photocatalysis of methylene blue: normalized concentration of MB as a function of time for In_2O_3 and In_2O_3/α-Fe_2O_3 thin film under solar radiation

Conclusion

On glass substrates, we effectively created In_2O_3/α-Fe_2O_3 thin films using an easy spray pyrolysis method. The rhombohedral structure of α-Fe_2O_3 and the cubic phase of In_2O_3 are confirmed by X-ray diffraction experiments; this conclusion was further supported by Raman spectroscopy. Scanning electronic microscopy (SEM) was used to analyze the surface morphology of In_2O_3/α-Fe_2O_3 thin film, and the results show that a fairly homogeneous surface with spherical grains of various sizes that are randomly disturbed has formed. The majority of the electrons in In_2O_3/α-Fe_2O_3 are free charge carriers, according to observations of the Hall effect. Charge carriers concentration, resistivity and Hall mobility are all identical to 5.7×10^{-4} Ω cm, 5.82 cm^2/V S and 1.87×10^{21} cm^{-3}, respectively. In contrast, for In_2O_3 and In_2O_3/α-Fe_2O_3 thin films, the grain size was equal to 28.2 nm and 30.61 nm, respectively. The photocatalytic activity for MB for these sprayed thin films is then assessed. It was discovered that the photocatalytic activity and degradation mechanism of the MB dye were affected by the paired In_2O_3/α-Fe_2O_3 photoatalysts.

Acknowledgements This work was funded by the Deanship of Graduate Studies and Scientific Research at Jouf University under grant no. (DGSSR-2023-02-02269).

Data availability We declare that all data are available in the manuscript file.

Declarations

Conflict of interest We declare that this manuscript is original and has not been published elsewhere nor is it currently under consideration for publication elsewhere. We also declare that this work was funded by the Deanship of Graduate Studies and Scientific Research at Jouf University under grant no. (DGSSR- 2023-02-02269).

References

1. Z. Najaf, D.L.T. Nguyen, S.Y. Chae, O.S. Joo, A.U.H.A. Shah, D.V.N. Vo, V.H. Nguyen, Q.V. Le, G. Rahman, Recent trends in development of hematite (α-Fe_2O_3) as an efficient photoanode for enhancement of photoelectrochemical hydrogen production by solar water splitting. Int. J. Hydrogen Energy **46**, 23334–23357 (2021)
2. B.C. Zhao, B. Xia, H.W. Ho, Z.C. Fan, L. Wang, Anamalous Hall effect in Cu and Fe codoped In_2O_3 and ITO thin films. Physica B Condens. Matter **404**, 2117–2121 (2009)
3. S. Kulaszewicz, W. Jarmoc, I. Lasocki, K. Turowska, Studies of the Hall effect in thin films SnO_2:Sb and In_2O_3:Sn films obtained by the hydrolysis method. Thin Solid Films **117**, 157–162 (1984)
4. D. Feng, J. Qu, R. Zhang, X. Sun, L. Zheng, H. Liu, X. Zhang, Z. Lu, F. Lu, W. Wang, H. Dong, Y. Cheng, H. Liu, R. Zheng, ITO regulated high-performance n-Si/ITO/α-Fe_2O_3 Z-scheme heterostructure towards photoelectrochemical water splitting. J. Catal. **381**, 501–507 (2020)
5. F. Baig, Y.H. Khattak, S. Jemai, B.M. Soucase, S. Beg, Hydrothermal synthesis of vanadium doped α-Fe_2O_3 cubic particles with enhanced photoelectrochemical activity. Sol. Energy **182**, 332–339 (2019)
6. F. Zhang, X. Li, Q. Zhao, Q. Zhang, M. Tade, S. Liu, Fabrication of composite hollow microspheres: a novel hybrid photocatalyst for toluene degradation under visible light. J. Colloid Interface Sci. **457**, 18–26 (2015)
7. M. Ivanovskaya, D. Kotsikau, A. Taurino, P. Siciliano, Structural distinctions of Fe_2O_3–In_2O_3 composites obtained by various sol gel procedures and their gas sensing features. Sens. Actuators B Chem. **124**, 133–142 (2007)
8. W. Smok, M. Zaborowska, T. Tanski, A. Radon, Novel In_2O_3/SnO_2 heterojuction 1D nanostructure photocatalyst for MB degradation. Opt. Mater. **139**, 113757 (2023)
9. M. Ivanovskaya, D. Kotsikau, G. Faglia, P. Nelli, Influence of chemical composition factors of Fe_2O_3/In_2O_3 sensors on their selectivity and sensitivity to ethanol. Sens. Actuators B Chem. **96**, 498–503 (2003)
10. X. Chi, C. Liu, L. Liu, S. Li, H. Li, X. Zhang, X. Bo, H. Shan, Enhanced formaldehyde-sensing properties of mixed Fe_2O_3–In_2O_3 nanotubes. Mater. Sci. Semicond. Process. **18**, 160–164 (2014)
11. L. Wu, S. Ma, J. Li, X. Li, In_2O_3 anchored Fe_2O_3 nanorod arrays for enhanced photoelectrochemical performance. Thin Solid Films **724**, 138600 (2021)
12. Z. Zhang, C. Gao, Y. Li, W. Han, W. Fu, Y. He, E. Xie, Enhanced charge separation and transfer through Fe_2O_3/ITO nanowire arrays wrapped with reduced graphene oxide for water splitting. Nano Energy **30**, 892–899 (2016)
13. S. Zhang, P. Song, Q. Wang, Enhanced acetone sensing performance of an α-Fe_2O_3–In_2O_3 heterostucture nanocomposite sensor. J. Phys. Chem. Solids **120**, 261–270 (2018)
14. N. Suzuki, K. Kaneko, S. Fujita, Growth of corundum structured In_2O_3 thin films on sapphire substrates with Fe_2O_3 buffer layers. J. Cryst. Growth **364**, 30–33 (2013)
15. P. Chang, Y. Wang, Y. Wang, Y. Zhu, Current trends on In_2O_3 based heterojuction photocatalytic systems in photocatalytic application. Chem. Eng. J. **450**, 137804 (2022)
16. Y. Xing, W. Que, X. Yin, Z. He, X. Liu, Y. Yang, J. Shao, L.B. Kong, In_2O_3/$Bi_2Sn_2O_7$ heterostructured nanoparticles with enhanced photocatalytic activity. Appl. Surf. Sci. **387**, 36–44 (2016)
17. X. Zhou, J. Wu, Q. Li, T. Zeng, Z. Ji, P. He, W. Pan, X. Qi, C. Wang, P. Liang, Carbon decorated In_2O_3/TiO_2 heterostructures with enhanced visible light driven photocatalytic activity. J. Catal. **355**, 26–39 (2017)
18. P. Luan, M. Xie, D. Liy, X. Fu, L. Jing, Effective charge separation in the rutile TiO_2 nanorods coupled Fe_2O_3 with exceptionally high visible activities. Sci. Rep. **4**, 6180 (2014)
19. Y. Li, Q. Wu, Y. Chen, R. Zhang, C. Li, K. Zhang, M. Li, Y. Lin, D. Wang, X. Zou, T. Xie, Interface engineering Z-scheme Ti-Fe_2O_3/In_2O_3 photoanode for highly efficient photoelectrochemical water splitting. Appl. Catal. B **290**, 120058 (2021)
20. N. Guo, H. Liu, Y. Fu, J. Hu, Preparation of Fe_2O_3 nanoparticles doped with In_2O_3 and photocatalytic degradation property for rhodamine B. Optik **201**, 163537 (2020)